Sinusoidal gold corrugation based plasmonic fiber-optic nano-tip refractive index sensor

D. KUMAR[1,2], J. B. MAURYA[1,*], R. RANJAN[1]
[1]*Department of Electronics and Communication Engineering, National Institute of Technology Patna, Bihar, 800005, India*
[2]*Department of Electronics and Communication Engineering, Graphic Era Hill University, Dehradun, Uttarakhand, 248002, India*

The Fiber-tip is layered by a gold sinusoidal corrugation which generates surface plasmons at metal-sample interface. At the optimized corrugation parameters, the performance parameters viz. shift in resonance wavelength, bandwidth, minimum reflectance, sensitivity, propagation length, and maximum field at metal-sample interface are calculated for each of the nine windows lying between 400–800 nm. $\Delta\lambda$ or sensitivity increases with the windows of higher frequency. Analysis suggests that sensor is best suited for last window, i.e., ~720 nm to ~760 nm with maximum sensitivity of 533 nm/RIU. The non-decaying field in sample enables the proposed sensor for deep analyte sensing.

(Received May 25, 2025; accepted October 10, 2025)

Keywords: Corrugation, Fiber-tip, Gold, Multiband, Refractive index, Sensitivity, Sensor, Surface plasmon

1. Introduction

In the ever-evolving landscape of sensor technologies, one breakthrough has been quietly revolutionizing the way we detect and analyze molecular interactions, environmental changes, and biological processes. Traditional sensors require biomarkers for analysis and take more time to get results. Optical biosensors outperform traditional sensors because they allow label-free sensing in real-time. Optical sensors are also more accurate than traditional sensors. SPR has emerged as a versatile technique, offering exceptional sensitivity and precision. When coupled with optical fiber and engineered into a fiber tip sensor, SPR opens up a world of possibilities for real-time monitoring, diagnostics, and quality control. SPR is a fascinating optical phenomenon that occurs when incident light interacts with a thin metal film making the interface with the dielectric medium. This interaction results in a shift in the resonance conditions, specifically the angle or wavelength of the incident light, due to changes in the refractive index of the adjacent medium. Therefore, SPR is exquisitely responsive to even the minutest alterations in the medium's refractive index, making it a highly sensitive sensing technique [1, 2]. The fusion of SPR with optical fiber in the form of a fiber tip sensor has unlocked a wide range of applications across diverse fields. By taking advantage of the inherent advantages of optical fiber, such as its flexibility, ability to transmit light over long distances, and immunity to electromagnetic interference, fiber tip SPR sensors have become invaluable tools in disciplines as varied as biomedical research, environmental monitoring, and chemical analysis. The intersection of optics and biotechnology has given rise to innovative sensing technologies, and among them, SPR-based optical biosensors have emerged as powerful tools for real-time and label-free detection of biomolecular interactions [3, 4].

The researcher proposed a different way of designing an SPR-based optical sensor. Various interrogation strategies are employed in optical sensors. The phase interrogation approach has been thoroughly investigated and has demonstrated remarkable results with higher resolution and dynamic range; yet it suffers from a complicated test setup, making it unsuitable for practical applications [5,6]. Another interrogation approach analyzes the intensity of transmitted or reflected light. The intensity interrogation method requires monochromatic light, making it simple and low-cost. However, the excitation wavelength is dependent on the materials employed in sensor fabrication [7,8]. Spectral interrogation is the most utilized approach in SPR-based sensors. This technique requires a broadband source.

A certain wavelength is absorbed from transmitted light, and the resonating wavelength shifts with the change in the sample refractive index. The shift in resonating wavelength is utilized for analysis. Sensors that use spectral interrogation are designed using a transmissive or reflective concept. Transmissive fibers are etched from the side, whereas reflective fibers have mirrored fiber tips, which reflect light back into the optical fiber. The fiber-tip-based optical sensors are compact in size and easy to use compared with transmissive sensors. The tip of the sensor is dipped in the sample and the reflected light in the fiber is used for measurement. The measurement setup can be developed as a low-cost, potent, and portable optical reader through the integration of prefabricated optical components such as a broadband light source, a coupler, and a spectrometer [1, 2, 7, 10].

In 2010, Yongbin Lin et al. proposed a gold nanodot array-based fiber tip sensor for LSPR biosensing with a sensitivity of 196 nm/RIU [11]. In 2012, Hsing-Ying Lin et al. fabricated a tapered fiber-based sensor having high sensitivity for biosensing applications [12]. In 2013, P. Uebel et al. proposed the fabrication of a gold nanotip attached to tapered optical fiber for plasmon-enhanced near-field detection. This structure utilizes the fiber tip for measurement but suffers from a complex measurement setup [13]. In 2014, Beniamino Sciacca and Tanya M. Monro proposed a multiplexed dip biosensor with gold and silver nanoparticles on the fiber tip [14]. In 2018, Alves et al. designed a metal-based fiber-optic corrosion sensor that shows a good response to corrosion. Authors used Aluminum as a metal as suggested to test other metals in future work in this field [15]. In 2020, Nidaa L. et al. fabricated and tested a multimode tip fiber sensor based on SPR. This simple sensor shows the linear shift in the dip at a longer wavelength with an increase in sample refractive index [16]. In 2022, Y. Zhang et al. fabricated a fiber-tip sensor for label-free bio-detection [17]. In 2022. In 2022, Alba Calatayud-Sanchez et al. fabricated tip based optical fiber LSPR sensor which requires characterization before their use [18]. In 2022, Hong Lei et al. proposed a fiber tip-based biosensor for the detection of food crop contaminates [19]. In 2025, Choi et al. showed label-free sensing of cancer exosomes by using nanostructured fiber tips, highlighting the diagnostic value of corrugated plasmonic probes [32]. In 2025, Špringer et al. have listed fiber-optic SPR sensors at the 700–800 nm window as the most important for point-of-care clinical translation [33]. In 2025, Singh et al. obtained real-time small-molecule sensing using meta surface enhanced SPR fibers, confirming deep-field penetration facilitated by sub-wavelength corrugations [34].

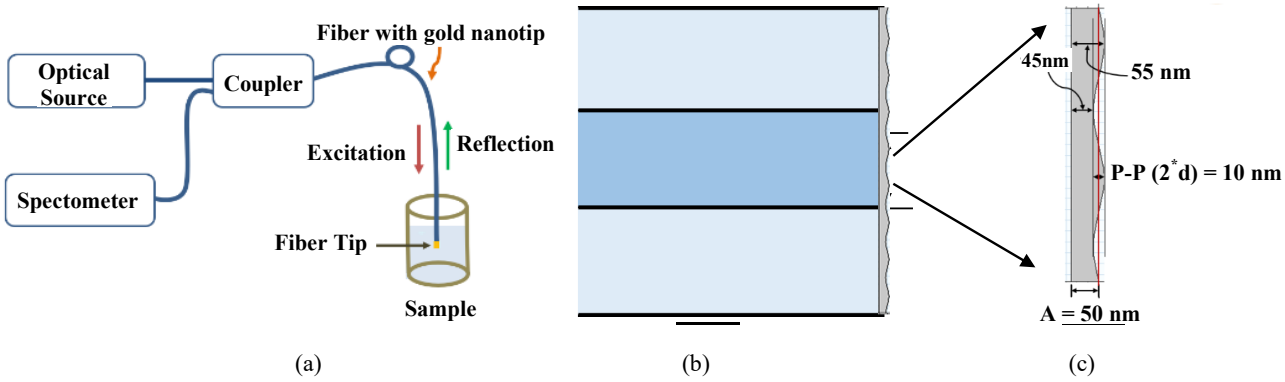

Fig. 1. (a) Measurement setup using fiber tip sensor (b) Structure of proposed fiber tip having corrugation at the metal layer (c) Magnified view to the corrugation at the metal surface (colour online)

In the Fiber-tip sensor, the metal coating on the fiber facet acts as a mirror, reflecting light back into the optical fiber. Modifying the surfaces of sensor with nanomaterials of various dimensions can enhance the overlap of electromagnetic field intensity in the analyte area. This modification can also bolster the interactions between plasmons and excitons, as well as the interactions between analyte molecules and metal surfaces [3]. Many researchers have worked on the fiber-tip sensor but most of them fabricated the sensor and have not done the numerical simulation. The nano-dot structure at the fiber end facet is used by them and none of the researcher used corrugation at the fiber end [20–26].

The proposed research on the fiber-tip sensor introduces several novelty points:

1. Application of sinusoidal corrugation at the fiber tip which generates multiple windows in the reflectance spectrum.
2. Multiple windows in the reflectance spectrum makes the proposed sensor flexible to use for different polychromatic laser
3. Far deep penetration depth in the sample enhances the interaction volume of SPW with the analyte.

2. Sensor design and performance parameter

2.1. Structure and theoretical modeling

The design of the proposed fiber-tip sensor is shown in Fig. 1. Fig. 1(a) shows the possible measurement process using a fiber-tip sensor to detect the change in sample refractive index. To obtain spectral information from a sample, a fiber tip can be inserted into it. Next, a broadband source can be coupled to the fiber, launching light through it. The fiber tip can be coated with a reflective corrugated metal film, which will reflect the light back into the fiber. The reflected light can be analyzed by a spectrometer, allowing for the observation of spectral characteristics of the sample. The optical fiber used in the system is a single-mode fiber with a core diameter of 8 µm and a cladding diameter of 125 µm. At the fiber facet, a thin layer of gold metal is applied with a corrugated surface. The corrugated surface helps to improve the coupling efficiency of the fiber and enables better control over the direction of the light beam. This type of configuration is commonly used in various optical systems where high precision and low loss transmission are required. Fig. 1(b) shows the structure of the proposed fiber tip. The corrugated metal layer is attached to a plain

fiber facet covering the entire fiber tip. In Fig. 1(c), a closer look at the fiber tip corrugation is presented. The width of the base metal, denoted as A, is measured to be 50 nm. At the metal surface, a sinusoidal profile with a corrugation of ±5 nm is used. This leads to an effective metal layer width that varies between 45 nm and 55 nm.

The wavelength dependent refractive index parameters for optical fiber are calculated using Sellmeier equation [10].

$$n(\lambda)=\sqrt{1+\frac{a_1\lambda^2}{\lambda^2-b_1^2}+\frac{a_2\lambda^2}{\lambda^2-b_2^2}+\frac{a_3\lambda^2}{\lambda^2-b_3^2}} \quad (1)$$

where λ is the operating wavelength, a and b are the Sellmeier coefficients for 3.1% GeO_2 dopped silica core and pure silica cladding. The values of these coefficients are listed in Table 1.

Table 1. Sellmeier coefficients for 3.1% GeO_2 dopped silica core and pure silica cladding

Coefficients	a_1	a_2	a_3	b_1 (μm)	b_2 (μm)	b_3 (μm)
Dopped silica core	0.7028554	0.4146307	0.8974540	0.0727723	0.1143085	9.896161
Pure silica cladding	0.6961663	0.4079426	0.8974794	0.0684043	0.1162414	9.896161

Silver and gold are frequently utilized as metal layers in SPR-based sensors because of their superior light absorption at resonance. Gold is preferred over silver because silver is prone to oxidation [27]. Wavelength-based metal layer complex permittivity is calculated using the Drude dispersion model [28].

$$\varepsilon_m(\lambda)=1-\frac{\lambda^2\lambda_c}{\lambda_p^2(\lambda_c+i\lambda)} \quad (2)$$

where, ε_m is the metal layer complex permittivity. λ, λ_C, and λ_P, are the operating wavelength, collision wavelength, plasma wavelength, respectively. For the gold metal layer, the value of λ_P is taken as 0.16826 μm and the value of λ_C is taken as 8.9342 μm [10].

2.2. Performance parameter

Enhancing the performance of fiber tip SPR sensors primarily focuses on specific parameters viz. sensitivity, Figure of Merit (FOM), penetration depth (PD) and propagation length (PL). The depth of the resonance dip depends on the energy coupling between the resonance Surface plasmon polaritons (SPP) modes and the evanescent wave. Greater coupling leads to a deeper dip which results in minimum reflection intensity at SPR. Meanwhile, the bandwidth of the resonance dip is prescribed by the gap between the coupling of resonance SPP modes with the evanescent wave and non-resonance SPP modes with the evanescent wave. A larger difference results in a narrower bandwidth. Bandwidth is determined as the difference between the corresponding wavelength where the reflection intensity is equal to half of the sum of maximum reflection intensity (R_{max}) and minimum reflection intensity (R_{min}) for each resonance dip. Here, R_{min} indicates maximum absorption of incident light in the metal which in effect maximizes the SPW.

2.2.1. Sensitivity

Sensor sensitivity (S) is characterized by the shift in resonance wavelength resulting from a unit change in sample refractive index and expressed as equation (3).

$$S=\frac{\Delta\lambda}{\Delta n} \quad (3)$$

where Δn is the change in sample refractive index which results in shift of resonating wavelength $\Delta\lambda$.

2.2.2. Figure of Merit

The figure of merit serves as a comprehensive quantitative indicator for assessing the sensor's performance and is expressed as equation (4).

$$FOM=\frac{S}{bandwidth\times(1-R)} \quad (4)$$

where, R is the reflection intensity.

2.2.3. Penetration Depth (PD)

In SPR sensors, the PD refers to how far the SPW extends into the medium from the metal surface. This can be measured graphically as a distance normal to metal-sample interface at which its intensity decays to (1/e) (about 37%) of its initial value at metal-sample interface.

2.2.4. Propagation Length (PL)

In SPR sensors, the PL refers to the distance over which the intensity of the SPW decays to (1/e) (about 37%) of its initial value. This decay occurs due to energy loss as the plasmon wave travels along the metal surface. This distance parallel to the sample metal interface is measured for PL.

2.3. Modeling using COMSOL

The numerical simulation of the proposed structure is done using COMSOL Multiphysics. Wave optics module is used with an electromagnetic wave, frequency domain as physics, and boundary mode analysis is performed to detect the reflection intensity at the numeric port. Standard single-mode fiber (SMF) having a core diameter of 8 μm

and a cladding diameter of 125 µm can be used for fabrication. However, in modeling, to get more accurate results with finer mesh, the cladding diameter is limited to 20 µm as the wave propagation length at metal-sample interface is less than 20 µm [6]. The fiber tip of 10 µm is used and the thickness of sample is taken as 3 µm. The wavelength dependent refractive indexes of fiber core, cladding and metal layers are calculated using equations 1, and 2. The structure is simulated for the sample refractive index of 1.33, 1.36 and 1.39 to cover large range of sample's refractive indices. The considered refractive indices of sample cover the bio samples, e.g., viruses, bacteria, lipids, protein etc., chemical samples, cancers cell, etc. The proposed sensor can be used for the detection of biomolecules, pathogens, and chemicals in blood, water, food, and air with deep penetration. Its multi-window flexibility suits portable diagnostics, environmental monitoring, industrial quality assurance and quality control. The mesh size for the metal layer and its boundaries is set to a maximum of 0.005 µm and minimum size of 0.0004 µm.

2.4. Fabrication and experimental possibilities

Fiber tip sensors have a wide range of fabrication possibilities due to their versatility and the variety that can be used in their construction. Many researchers have fabricated the fiber tip using gold nano-dot at the surface [11 – 19]. The proposed sensor can be fabricated by first cleaving and cleaning a single-mode fiber, then sputtering a 50 nm gold layer (with a 2–3 nm chromium (Cr) and/or titanium (Ti) adhesion film) onto its facet. A sinusoidal corrugation (≈ 0.5 µm pitch, ≈ 5 nm amplitude) can be patterned into the gold using either focused-ion-beam milling, nano-imprint lithography, or laser-interference lithography. After rinsing and optional plasma cleaning, the fiber can be coupled to a broadband source and spectrometer for refractive index sensing as shown in Fig. 1(a). Though it is not possible to fabricate the proposed structure with 100% accuracy of the corrugation profile, results of the simulation showed that if there is a small deviation in the corrugation profile then still it does not have deviations in the resonant wavelengths.

3. Results and discussions

The metal layer is 50 nm thick at the fiber tip; however, given the corrugation, the effective metal layer thickness varies depending on the corrugation profile. A sinusoidal profile is chosen for corrugation. In Fig. 2(a), the influence of amplitude variation is investigated to determine the optimal amplitude of corrugation. For this investigation, a sample with a refractive index of 1.33 was used. The results indicate that changes in the corrugation's amplitude cause variations in the SPR dip. It is confirmed that altering the corrugation's amplitude does not cause a change in the resonating wavelength. There are variations in the resonance dip profile. Weak surface plasmon coupling is observed for plane metal surfaces.

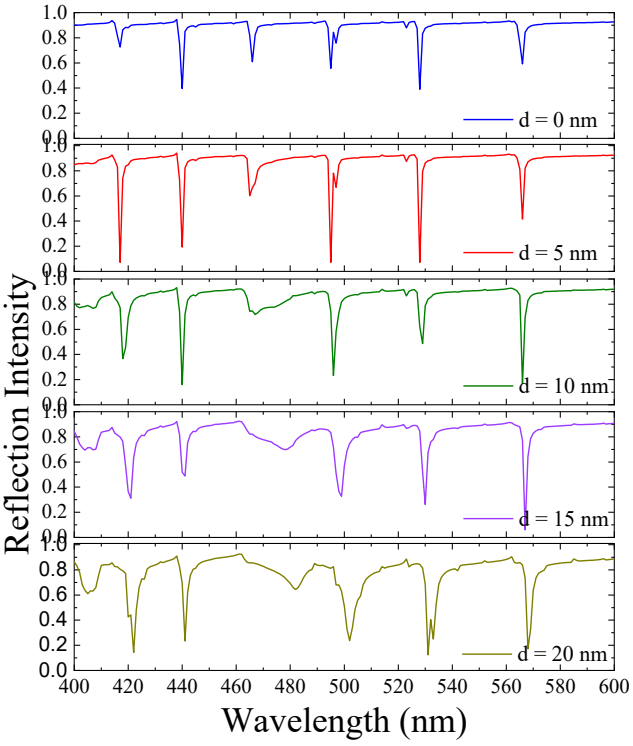

(a)

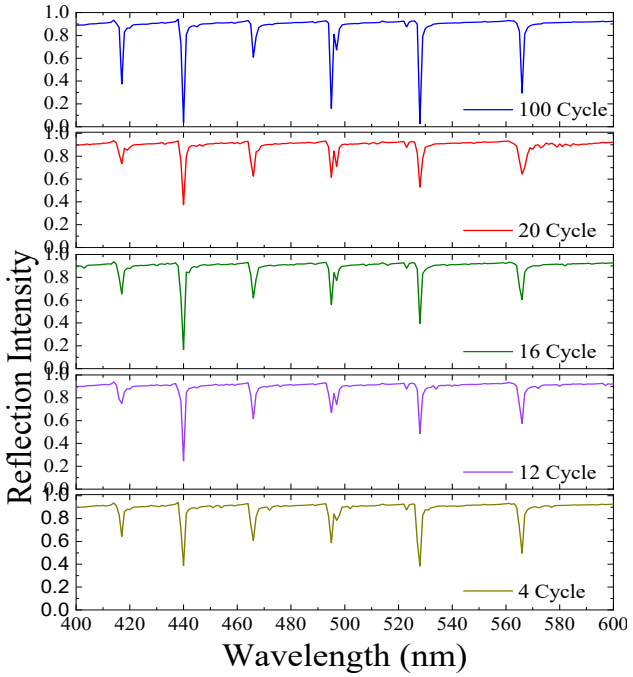

(b)

Fig. 2. (a) Reflection intensity with change in roughness amplitude of 0 nm, 5 nm, 10 nm, 15 nm, and 20 nm on metal layer (A) of 50 nm with the sample having a refractive index (N_S) of 1.33 (b) Reflection intensity with change in roughness periodicity (metal layer thickness = 50 nm, roughness amplitude = 5 nm and sample refractive index (N_S) = 1.33) (colour online)

Following corrugation induction, there was an improvement in light absorption at the resonance wavelength. The reflectance dips are getting broader with the corrugation amplitude. A corrugation amplitude of 5 μm is opted for the sake of sharper dip and lower minimum reflectance.

Since a sinusoidal corrugation profile is adopted, the impact of the corrugation period on the intensity of reflection at SPR is also looked at and the results are shown in Fig. 2(b). For this analysis, a 50 nm metal layer with a 5 μm roughness amplitude is used. The sample refractive index is taken as 1.33. The number of cycles in the core region is set at four, twelve, sixteen, and one hundred. The results reveal that there is no shift in the resonating wavelength due to a change in corrugation frequency. There is a minor difference in the reflection intensity as the period changes. Roughness with higher periodicity will also be more difficult to fabricate because the sinusoidal shape may be converted to triangular shape. Therefore, the optimal corrugation periodicity is 16 cycles in the core region.

After optimizing the corrugation amplitude and periodicity, the fiber tip was tested to detect changes in the sample's refractive index. The effect of the change in sample refractive index is investigated using a 50 nm thick corrugated metal layer with a corrugation amplitude of 5 nm and a corrugation period of 0.5 μm (16 cycles in the core area). Refractive indices of 1.33, 1.36, and 1.39 are utilized as sample values. The outcomes are displayed in Fig. 3(a). A red shift is observed as the sample refractive index increases.

The linear shift in the wavelength is linear with change in the sample refractive index. There are different measurement windows. Nine windows are observed in the 400–800 nm wavelength range. These windows are shown in Fig. 3(a) as W_1, W_2, W_3, W_4, W_5, W_6, W_7, and W_9.

These windows are selected based on reflectance dips obtained corresponding to sample's refractive indices, i.e., 1.33, 1.36, and 1.39 at different wavelengths. The measurement can be carried out with any of the nine windows.

The comparison of wavelength shift, bandwidth, minimum reflection intensity changes, propagation length and maximum electric field intensity at metal sample interface for each of the nine measurement windows are displayed in Fig. 3(b). It was observed that the shift in SPR wavelength is linear towards higher wavelength as the refractive index varied from 1.33 to 1.36 and 1.33 to 1.39. As the refractive index increases, the wavelength shift also increases at higher wavelengths. Generally, the reflectance dips show shallowing nature with red shift at longer wavelengths. The reflectance dips are becoming broader at lower as well as higher wavelengths with the increase in sample refractive index.

In 1978, Pockrand investigated the dispersion relation of SPR at metal surfaces, verifying the effect of shallowing and broadening [9]. Since the radius of the fiber core is 4 μm and the average propagation length is around 3.5 μm, the propagation length analysis demonstrates the better field confinement.

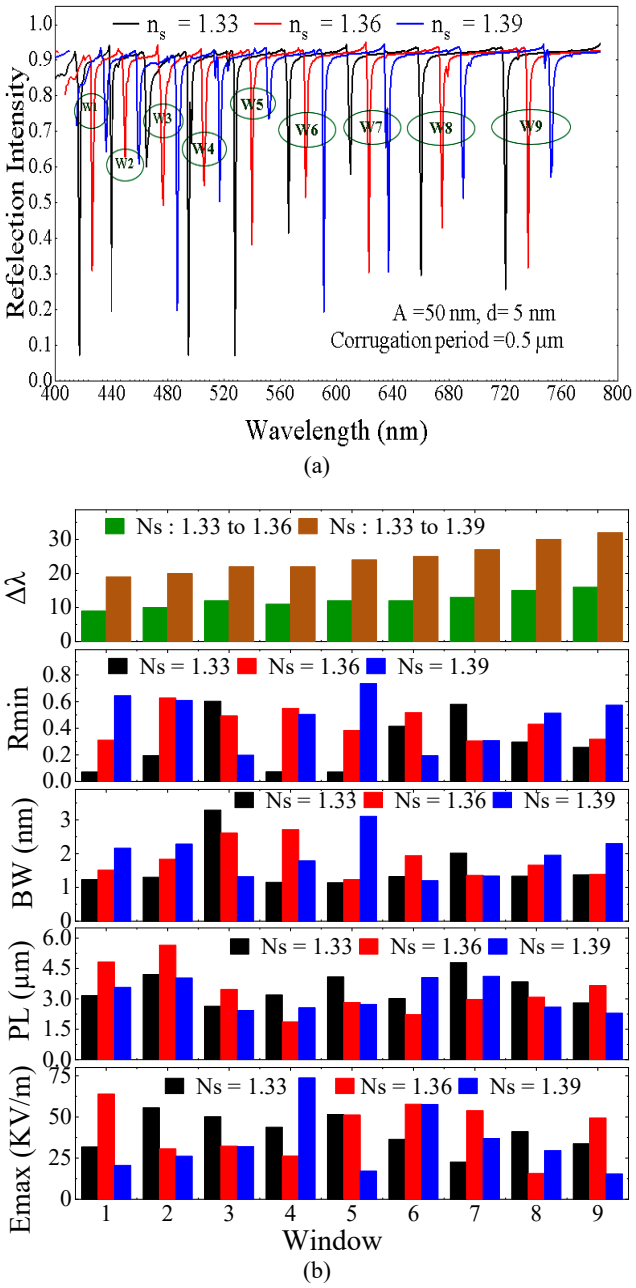

Fig. 3. (a) Reflection intensity with change in sample refractive index having metal layer roughness amplitude of 5 nm and corrugation period of 0.5 μm (b) Comparison of the change in wavelength (Δλ) with change in RI, minimum reflection intensity (Rmin), bandwidth, PL and Maximum electric field intensity in sample at metal sample interface in all measurement windows (colour online)

The PL analysis for the suggested fiber tip is displayed in Fig. 4. Fig. 4(a) depicts the electric field in the fiber core and sample, while Fig. 4(b) provides an enlarged view of the metal sample contact. The field is transmitted at resonance in the sample region and is well-confined in the core region. The electric field fluctuation with respect to the displacement from the core center is depicted in Fig. 4(c). The intensity of the electric field reaches its maximum at the core's center and decreases

with distance in the direction of the cladding. The electric field behaves in an oscillating pattern. The red curve depicts the envelope of electric field intensity fluctuations. The PL of 4.2 µm is graphically calculated. The envelope in Fig. 4(c) shows many peaks. However, the central peak is significant because it lies in the core having high intensity. Whereas, the peaks lying in the cladding will less participate in the sample detection because of its very low intensities with respect to central peak. Therefore, PL is calculated corresponding to central peak.

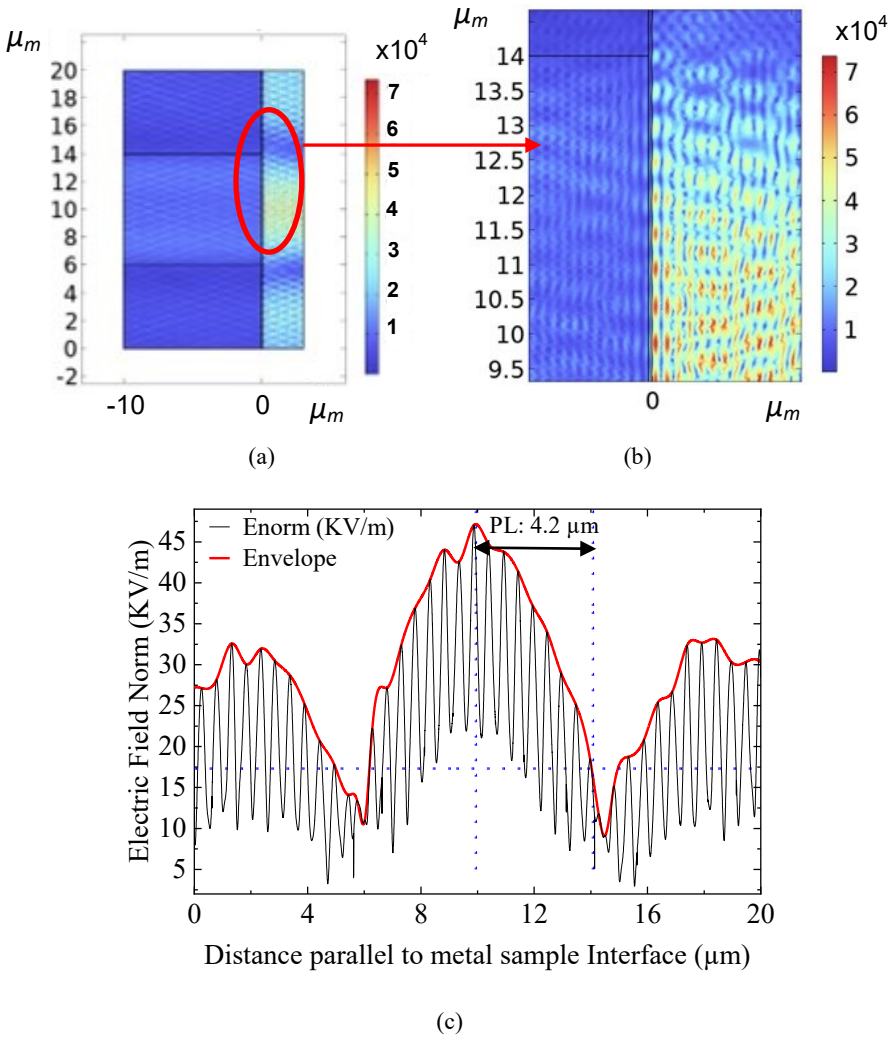

Fig. 4. PL at wavelength of 440 nm with sample refractive index of 1.33 (a) Electric field in core and sample at resonance (b) Magnified view (c) Electric field intensity with change in the distance from fiber core

Fig. 5 shows the electric field in the fiber core and sample for the analysis of PD. The electric field intensity variation in the sample and core is shown in Fig. 5(a). For the simulation, a 3 µm-long sample is used, and the outcome reveals a non-decaying field pattern. After extending the sample's length to 200 µm, in Fig. 5(b), it was discovered that the intensity of the electric field does not decrease considerably with distance.

The improved light transmission into the sample is a result of the higher PD, which maximizes the interaction between the evanescent wave and the surface plasma wave.

The sample size has no bearing on the sensor's response. Therefore, this non-decaying behavior of electric field in the sample enables the proposed sensor to be used for deep analyte sensing.

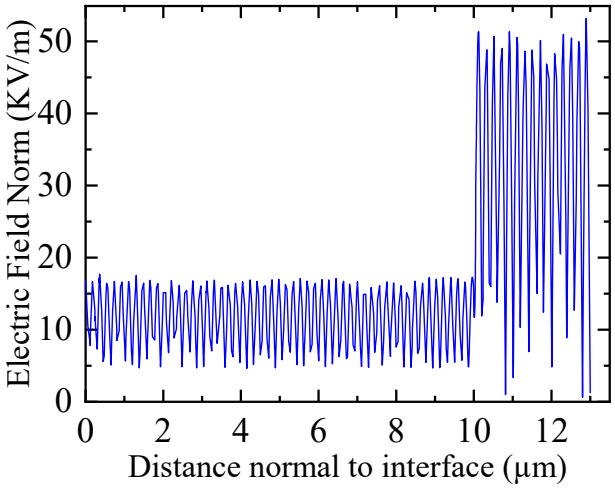

(a)

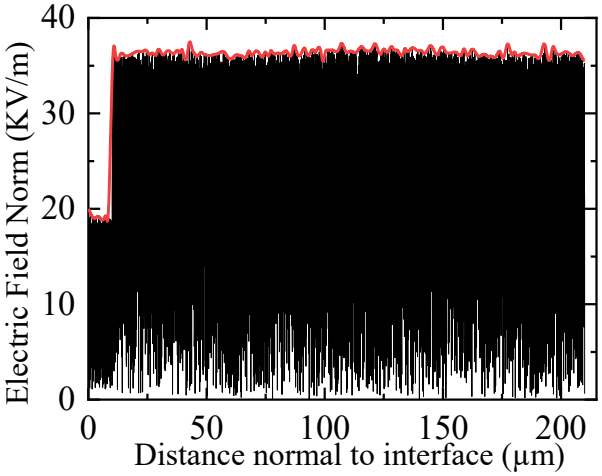

(b)

Fig. 5. Electric field intensity variation along the center of the fiber core and sample (a) Electric field intensity variation in core and sample with sample length of 3 μm (normal to the metal sample interface) (b) Electric field intensity variation in core and sample with sample length of 200 μm (normal to the metal sample interface) (colour online)

Fig. 6 illustrates how sensitivity changes with change in sample refractive indexes and windows. Sensitivity increases as the operating wavelength increases. The maximum sensitivity of 533.3 nm/RIU is achieved at a wavelength of roughly 750 nm.

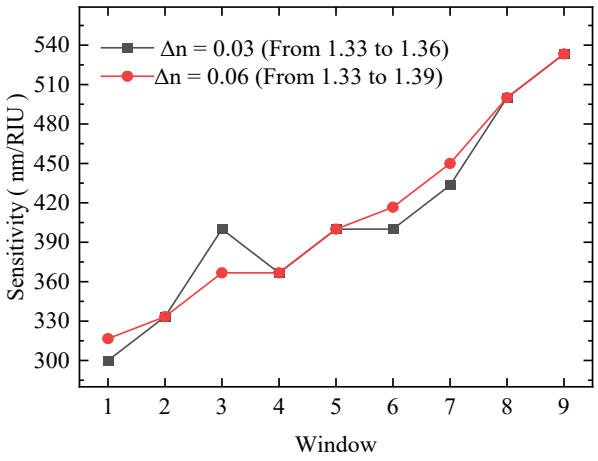

Fig. 6. Sensitivity with change in sample refractive index from 1.33 to 1.36 and 1.33 to 1.39 (colour online)

To clearly showcase the innovation and benefits of the proposed fiber tip sensor, Table 2 provides a comparison of the proposed fiber tip sensor with the previously reported spectral back-reflect SPR fiber optic tip sensors. The proposed corrugated metal film probe exhibits superior sensitivity compared to the previously reported sensing tips.

Table 2. Sensitivity comparison of spectral back-reflect SPR fiber optic tip sensors

Ref.	Year	Resonant Structure	Fiber	S_λ (nm/RIU)
[11]	2010	Gold nanodot array	SMF Fiber Tip	196
[2]	2015	Ag nanoparticles	MMF Fiber Tip	387
[14]	2018	Au-Ag nanoparticles	MMF Fiber Tip	387
[16]	2020	Au thin film	MMF Fiber Tip	298
[29]	2020	Au nanodisk array	SMF Fiber Tip	188
[17]	2022	Au nanoparticles	MMF Fiber Tip	371
[30]	2023	Au nanodisk array/thin film	MMF Fiber Tip	138
[31]	2024	Bragg grating and Au thin film	SMF Fiber Tip	300
This Work	-	Corrugated Au thin film	SMF Fiber Tip	**533**

4. Conclusion

In this work, we presented numerical simulation of reflectance in fiber tip sensors that have sinusoidal corrugation at the fiber facet. Due to the corrugation, the light at the SPR wavelength is absorbed and transmitted into the sample resulting in minimum reflection at the input port. The transmitted light doesn't decay in the

sample enabling deep analyte sensing application of the proposed sensor. The proposed sensor showed multiple windows in its reflectance spectrum. A good response to changes in a sample's refractive index, with a sensitivity of 533 nm/RIU is obtained in the windows ranging from ~720 nm to ~760 nm. The proposed sensor is flexible to operate in different range of frequency generated from polychromatic laser. This allows users to utilize the resources that best fit their specific needs.

Funding

This work was supported by the Science & Engineering Research Board (SERB), Department of Science & Technology, Government of India [FILE NO. SRG/2021/00l744].

Disclosures

The authors declare no conflicts of interest.

Data availability statement

No data was generated or analyzed in the presented research.

References

[1] J. Homola, Chem. Rev. **108**(2), 462 (2008).
[2] E. Klantsataya, P. Jia, H. Ebendorff-Heidepriem, T. M. Monro, A. Francois, Sensors **17**(1), 12 (2017).
[3] J. Jing, K. Liu, J. Jiang, T. Xu, S. Wang, J. Ma, Z. Zhang, W. Zhang, T. Liu, Photon. Res. **10**, 126 (2022).
[4] S. Lee, H. Song, H. Ahn, S. Kim, J. R. Choi, K. Kim, Sensors **21**(3), 819 (2021).
[5] C. Zhu, Y. Zhuang, B. Liu, J. Huang, IEEE Trans. Instrum. Meas. **71**, 7008212 (2022).
[6] A. Leung, P. M. Shankar, R. Mutharasan, Sensors and Actuators B: Chemical **125**, 688 (2007).
[7] F. Yesilkoy, Sensors **19**(19), 4287 (2019).
[8] Z. Yin, X. Jing, IEEE T. Instrum. Meas. **72**, 1 (2023).
[9] I. Pockrand, Surf. Sci. **72**(3), 577 (1978).
[10] A. R. Kadhim, L. Yuan, H. Xu, J. Wu, Z. Wang, IEEE Sens. J. **20**(17), 9816 (2020).
[11] Y. Lin, Y. Zou, Y. Mo, J. Guo, R. G. Lindquist, Sensors **10**(10), 9397 (2010).
[12] H. Y. Lin, C.H. Huang, G. L. Cheng, N. K. Chen, H. C. Chui. Opt. Express **20**(19), 21693 (2012).
[13] P. Uebel, S. T. Bauerschmidt, M. A. Schmidt, P. St. J. Russel, Appl. Phys. Lett. **103**(2), 021101 (2013).
[14] B. Sciacca, T. M. Monro, Langmuir **30**(3), 946 (2014).
[15] H. P. Alves, J. F. Nascimento, E. Fontana, I. J. Coêlho, J. F. Martins-Filho, J. Lightwave Technol. **36**(13), 2597 (2018).
[16] A. J. Nidaa, A. D. Anwaar, Sustainable Engineering and Innovation **2**, 10 (2020).
[17] Y. Zhang, H. Wu, H. Wang, B. Yin, S. H. D. Wong, A. P. Zhang, H. Y. Tam, Biosens. Bioelectron. **218**, 114761 (2022).
[18] A. Calatayud-Sanchez, A. Ortega-Gomez, J. Barroso, J. Zubia, F. Benito-Lopez, J. Villatoro, L. Basabe-Desmonts, Sci. Rep. **12**(1), 9566 (2022).
[19] H. Lei, C. Chen, H. Yan, IEEE Sens. J. **22**(18), 17838 (2022).
[20] F. Mumtaz, M. Roman, B. Zhang, L. G. Abbas, M. A. Ashraf, M. A. Fiaz, Y. Dai, J. Huang, IEEE Photonics J. **14**(5), 1 (2022).
[21] S. M. A. Uddin, S. S. Chowdhury, E. Kabir, Plasmonics **16**(6), 2025 (2021).
[22] L. Li, Y.-N. Zhang, IEEE T. Instrum. Meas. **70**, 1(2021).
[23] S. Vasudevan Pillai Radha, S. K. Santhakumari Amma Ravindran Nair, S. Sankaranarayana Iyer, ACS Omega **6**(23), 15068 (2021).
[24] F. Depiereux, N. Konig, T. Pfeifer, R. Schmitt, IEEE T. Instrum. Meas. **56**(6), 2279 (2007).
[25] X. Zhou, X. Li, S. Li, X. Yan, X. Zhang, F. Wang, T. Suzuki, Y. Ohishi, T. Cheng, IEEE T. Instrum. Meas. **70**, 1 (2021).
[26] S. Farhadi, M. Miri, A. Farmani, Sci. Rep. **11**(1), 21692 (2021).
[27] Y. Al-Qazwini, A. S. M. Noor, P. T. Arasu, A. R. Sadrolhosseini, Current Appl. Phys. **13**(7), 1354 (2013).
[28] S. Singh, B. D. Gupta, Meas. Sci. Technol. **21**(11), 115202 (2010).
[29] Y. Hong, D. Zhao, J. Wang, J. Lu, G. Yao, D. Liu, H. Luo, Q. Li, M. Qiu, Nano Lett. **20**(12), 8841 (2020).
[30] H. He, X. Wei, Y. He, Y. Liang, Y. Fang, W. Peng, Sensors **23**(8), 4163 (2023).
[31] S. N. Jouybari, M. G. Asl, S. M. Mousavi, Photon. Nanostr. - Fund. Appl. **63**, 101340 (2025).
[32] Choi, B. Dae, Maria L. García, L. Wei, A. H. Zewail, N. J. Halas, Light Sci. Appl. **14**, 177 (2025).
[33] T. Špringer, A. M. Spehar, J. R. Lu, H. Uji-i, L. Fabris, Biosensors & Bioelectronics **278**, 117308 (2025).
[34] S. Singh, P. R. Shah, M. A. González, C. Zhang, O. Ilic, Biosensors **15**(2), 80 (2025).

*Corresponding author: jbm.ec@nitp.ac.in